

Comments on “Atlantic Tropical Cyclogenetic Processes during SOP-3 NAMMA in the GEOS-5 Global Data Assimilation and Forecast System”

SCOTT A. BRAUN

Laboratory for Atmospheres, NASA Goddard Space Flight Center, Greenbelt, Maryland

(Manuscript received 2 February 2010, in final form 11 March 2010)

1. Introduction

Considerable attention has been given to the potential negative impacts of the Saharan air layer (SAL) in recent years (Dunion and Velden 2004; Jones et al. 2007; Wu 2007; Dunion and Marron 2008; Reale et al. 2009, hereafter RL1; Shu and Wu 2009; Sun et al. 2008, 2009). Braun (2010) recently raised questions about the negative impacts of Dunion and Velden (2004) and other studies in terms of storms that reached at least tropical storm strength and suggested that the SAL was an intrinsic part of the tropical cyclone environment for both storms that weaken after formation and those that intensify. Braun (2010) also suggested that several incorrect assumptions underlie many of the studies on the negative impacts of the SAL, including assumptions that most low-to-midlevel dry tropical air is SAL air, that the SAL is dry throughout its depth, and that the proximity of the SAL to storms struggling to intensify implies some role in that struggle. The recent paper RL1 is an example of the problems inherent in some of these assumptions. In their paper, RL1 analyze a simulation from the Global Earth Observing System (GEOS-5) global model and describe an extensive tongue of warm, dry air (see the white and yellow shading in their Fig. 5) that stretches southward from at least 30°N (the northern limit of their plots) and wraps into a low pressure system during the period 26–29 August 2006, suppressing convection and possibly development of the African easterly wave associated with that low pressure system. They attributed the warm, dry tongue to the SAL (i.e., heating of the air mass during passage over the Sahara and radiative warming of the dust layer). Whether it was their intention, the implication is that *this entire feature*

is due solely to the SAL and not to other possible sources of dry air or warmth. In addition, they suggested that a cool tongue of air in the boundary layer located directly beneath the elevated warm, dry tongue (forming a thermal dipole) was possibly the result of reduced solar radiation caused by an overlying dust layer. They stated that “the cool anomaly in the lower levels does not have any plausible explanation relying only on transport.”

In this comment, evidence from satellite and global meteorological analyses is presented that casts considerable doubt upon RL1’s interpretation of the GEOS-5 forecasts and their conclusion that the results implied a negative role of the SAL. We show that the major portion of the warm, dry air aloft was located in a nearly dust-free slot between two Saharan dust outbreaks, had a significant source from the midlatitudes ($>30^{\circ}\text{N}$), and was likely driven by strong subsidence warming and drying. In addition, when wind fields are examined in a reference frame moving with the wave (Dunkerton et al. 2009), National Centers for Environmental Prediction (NCEP) global meteorological analyses suggest that the cool tongue in the boundary layer can be readily explained by transport of cooler air from higher latitudes. At the very least, it offers a plausible alternative explanation for the cool tongue that does not rely on radiative impacts of the dust.

2. Data

This comment makes use of level-3 (1° gridded) aerosol optical depth (AOD) data from the Moderate Resolution Imaging Spectroradiometer (MODIS) instruments on the National Aeronautics and Space Administration (NASA) *Terra* and *Aqua* satellites, which provide information on the concentration of aerosol within the column that are a clear indicator of SAL air. Tropical Rainfall Measuring Mission (TRMM) multisatellite-derived rainfall rates (Huffman et al. 2007) available at 0.25° horizontal resolution and 3-h temporal resolution are used to determine

Corresponding author address: Dr. Scott A. Braun, NASA GSFC, Mail Code 613.1, Greenbelt, MD 20771.
E-mail: scott.a.braun@nasa.gov

daily rainfall accumulations. Retrieved thermodynamic profiles of atmospheric temperature and relative humidity from Atmospheric Infrared Sounder (AIRS) and Advanced Microwave Sounding Unit (AMSU) level-2 (45-km resolution) products are used to characterize the vertical and horizontal thermodynamic structure of SAL and non-SAL air masses. Thermodynamic data are available at 12 pressure levels¹ in the troposphere, with the temperature data corresponding to the temperature at the pressure level, but with the relative humidity corresponding to the average between the specified level and the next level above. The AIRS-retrieved profiles of temperature and humidity are likely to be impacted by the radiative effects of dust. However, this impact has not yet been well characterized. Comparison of the AIRS profiles to dropsondes obtained during a NASA DC-8 flight on 26 August 2006—during the NASA African Monsoon Multidisciplinary Activities (NAMMA) field campaign—Global Forecast System (GFS) analyses, and NASA Modern Era Retrospective Analysis for Research and Applications (MERRA) analyses (not shown) indicates good consistency in all the respects discussed in section 3, suggesting that dust impacts likely do not affect the interpretations presented herein. To provide additional meteorological context for this event, final global meteorological analyses from the NCEP GFS are used. The analyses have 1° horizontal resolution and 6-hourly temporal resolution. The primary application of the GFS analyses is the computation of 6-day backward air trajectories at every grid point within the region 0°–40°N, 3°–60°W at 950, 850, 700, 600, 500, and 400 hPa for the period 21–28 August 2006 (although only results for 24–26 August and for 700 hPa will be shown). The trajectories are used to distinguish SAL and non-SAL air masses based on whether the air parcels pass over the Sahara at any time during the trajectories. In addition, the trajectories are used to determine the latitude and longitude of the origins of the air particles (i.e., if t_0 is the time the trajectories are released, then the origin latitudes and longitudes are the locations of the particles at t_0 minus 6 days, or t_{0-6}) and the amount of ascent or descent that occurred during the 6 days of the trajectory period.

3. Was the SAL responsible for the elevated warm, dry tongue and cool air beneath?

RL1 describe the supposed suppression of development of a tropical wave by Saharan air. Figure 1 depicts the evolution of the wave and Saharan dust using MODIS AODs, TRMM multisatellite-derived rainfall rates, and

GFS 700-hPa wave-relative streamlines between 25 and 28 August.² The tropical wave that is the focus of RL1 is located at the African coast on 25 August (Fig. 1a) with precipitation extending southward along the coast from the center toward the intertropical convergence zone (ITCZ). The mean motion (7.8 m s^{-1} to the west) of the wave, defined by the 700-hPa geopotential-height minimum between 25 and 28 August, is used to determine the wave-relative winds. On 25 August (Fig. 1a), a significant outbreak of dust (labeled SAL1) that had moved off of Africa several days earlier is just to the east and southeast of Tropical Storm Debby (23°N, 43°W). A new outbreak of dust (labeled SAL2) is readily apparent just west of the African coast while a low-dust or nearly dust-free tongue of air is seen between the two dust outbreaks to the northwest of the low pressure system. The wave-relative flow in the low-dust region is northwesterly, apparently bringing low-dust subtropical air southward between the two dust layers. The warm, dry tongue discussed by RL1 was coincident with this very low-dust or nearly dust-free tongue of air located between the two SAL outbreaks, as will be shown later (see Figs. 2 and 3).

On August 26 (Fig. 1b), the first dust outbreak is well to the south-southeast of a dissipating Tropical Storm Debby (~26°N, 47°W), with low-to-moderate AOD values (0.2–0.5), while the second outbreak contains very high AOD values (>0.8) near 25°N extending from the African coast westward to 30°W and lower AOD values extending southward to approximately 15°N. The AOD depression between SAL1 and SAL2 extends farther to the southwest and south of SAL2 as northwesterly and westerly wave-relative flow transports low-dust air into this region. Weak precipitation continues to occur on the northern side of the low pressure system, in the southern portion of the dust of SAL2. Additional precipitation occurs to the south of the low along the ITCZ.

Coincident data from AIRS and the Cloud–Aerosol Lidar and Infrared Pathfinder Satellite Observations (CALIPSO) near 0430 UTC 26 August confirm the general lack of dust within the elevated dry tongue (Fig. 2).

² Reale and Lau (2010) criticize the clarity of Fig. 1, including the low resolution (1°) of the MODIS AOD product and the NCEP analyses and the large domain that it shows, arguing that only large-scale features can be seen. Their argument has little validity, however. First, the main point of the figure is to demonstrate the large-scale evolution of multiple dust outbreaks, the nearly dust-free gap in between, and their relationship to the large-scale flow. Second, while the figure depicts the evolution of the dust on larger scales, all of the features are well resolved and readily apparent, including the dust boundaries. Unlike model fields, where certain scales are unresolved by the grid, the MODIS observations represent the average AOD within the 1° grid box, thereby incorporating information at smaller scales.

¹ AIRS retrieval levels are at 1000, 925, 850, 700, 600, 500, 400, 300, 250, 200, 150, and 100 hPa.

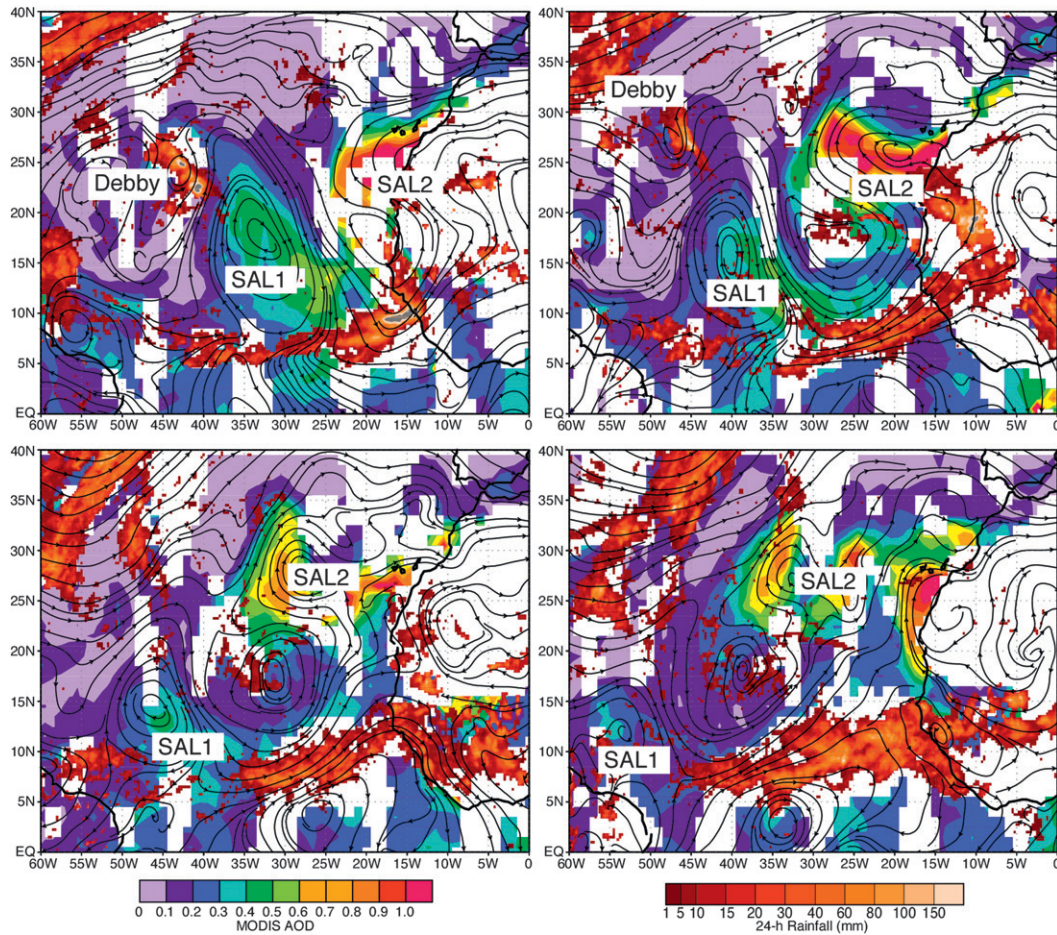


FIG. 1. MODIS level-3 AOD (bottom left color scale) averaged from *Terra* and *Aqua* at \sim 1400 UTC, TRMM multisatellite 24-h accumulated rainfall (bottom right color scale), and NCEP GFS 700-hPa storm-relative streamlines (mean westward storm motion of 7.8 m s^{-1}) at 1200 UTC (a) 25 Aug, (b) 26 Aug, (c) 27 Aug, and (d) 28 Aug 2006. White shaded regions depict areas of missing MODIS data. Tropical Storm Debby and the SAL dust outbreaks described in the text are labeled. Axis labels indicate latitude and longitude values.

The nighttime overpass is used because CALIPSO data quality is best at night. Because MODIS dust data are only available during afternoon overpasses (12 h before or later), the approximate MODIS dust boundary is estimated from an isochrone analysis of the MODIS dust data, linearly interpolating between the $\text{AOD} = 0.2$ isochrones at \sim 1640 UTC 25 and 26 August. The CALIPSO overpass crosses through SAL1 to the south of 20°N and through the middle of the dry tongue from 20°N and northward. A thick layer of dust is present in the CALIPSO data above the boundary layer south of 20°N . Beginning near 18°N , the top of the northern edge of the dust layer quickly lowers from an altitude of approximately 5 to 2.5 km before the dust layer ends at 20°N . Within the very dry air, little or no aerosol is found above the boundary layer, in agreement with the approximate MODIS dust boundary. The exact position of this boundary is not critical to the argument because

the CALIPSO overpass is clear in showing no dust within this portion of the dry air mass.

The general pattern from MODIS dust and GFS wave-relative streamlines continues into 27 (Fig. 1c) and 28 August (Fig. 1d) as the nearly dust-free ($\text{AOD} < 0.2$) tongue of air between SAL outbreaks expands and dominates the area of the wave. Small dust amounts ($\text{AOD} \approx 0.2\text{--}0.3$) can be seen advecting around the northwestern side of the circulation, suggesting the ingestion of SAL air at some level. Precipitation remains weak and scattered on the northern side of the low pressure center while ITCZ convection remains active well to the south. To summarize the information in Fig. 1, the MODIS data suggest back-to-back dust outbreaks gradually split apart by a tongue of increasingly low-dust or dust-free air, which is taken as an indication of the erosion or replacement of dusty SAL air by nondusty non-SAL air from the north and west. As will be shown next, this tongue of low or nearly dust-free air is

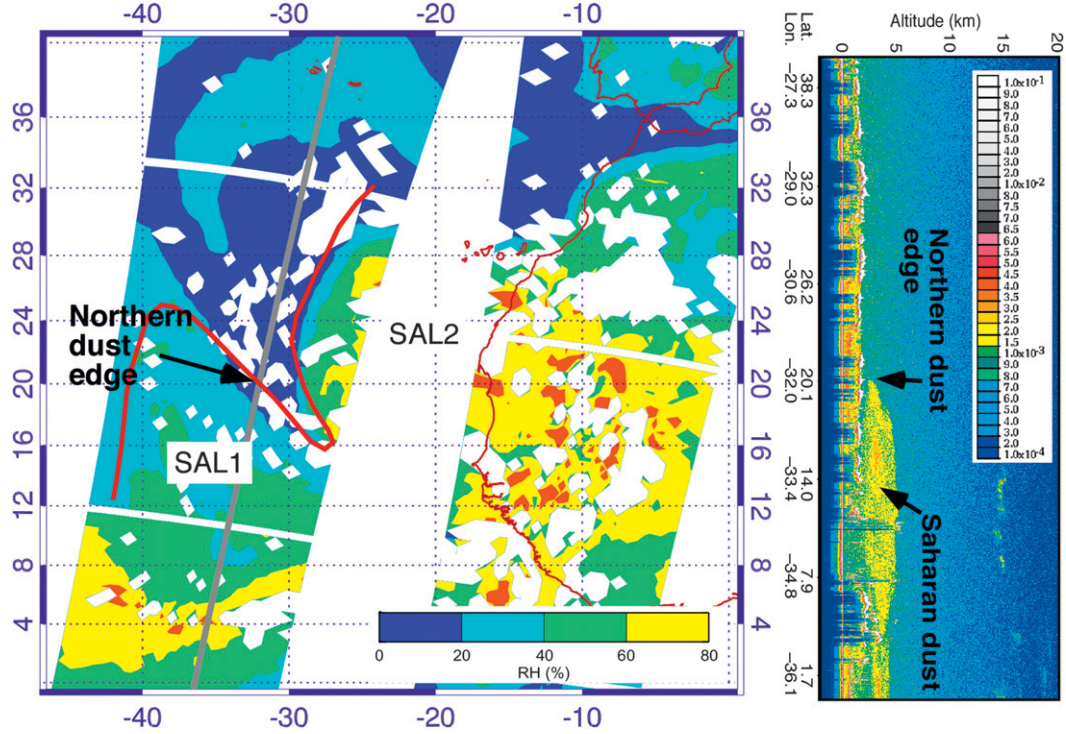


FIG. 2. (left) Level-2 AIRS/AMSU-derived 700–600-hPa layer relative humidity from descending orbits occurring at 0130 LT (~0430 UTC) 26 Aug. The approximate MODIS dust boundary at ~0430 UTC 26 Aug is indicated by the red line. The gray line indicates the track of the CALIPSO overpass. The two SAL outbreaks discussed in the text are labeled SAL1 and SAL2. Axis labels indicate latitude and longitude values. (right) CALIPSO 532-nm total attenuated backscatter ($\text{km}^{-1} \text{ sr}^{-1}$) at ~0430 UTC 26 Aug. The latitude and longitude of the subsatellite point are shown on the vertical axis; altitude is on the (top) horizontal axis.

collocated with the elevated warm, dry tongue of air and cooler boundary layer air described by RL1.

For the sake of brevity, Fig. 3 will focus on data on 27 August but is representative of other days during this event. Figure 3 shows AIRS/AMSU-derived temperature (relative humidity) for three levels (layers) extending from the base to near the top of the SAL. The primary dust regions are indicated by coincident-in-time MODIS dust data (red outlines; thick line, AOD = 0.2; thin line, AOD = 0.4), with the southern dust region labeled SAL1 and the northern dust region labeled SAL2, as in Fig. 1c. At 850 hPa (Fig. 3a), the warmest temperatures over the eastern Atlantic are within SAL2, with temperatures diminishing to the west within the dust boundaries. This pattern is a clear indication of the low-level warming that typically occurs as the air passes over the Sahara. The coolest temperatures are in a curving band (see the low-level cool anomaly in Fig. 8 of RL1) extending southward in advance of SAL2 into the low-dust region between the two SAL regions. These cooler temperatures represent the cool tongue at the top of the boundary layer and are representative of temperatures found at lower levels in the AIRS product. The relative humidity in the 850–700-hPa layer (Fig. 3b) is lowest to the north of SAL2

(<20%), with dry (<40%) air curving around the western border of SAL2 into the region between the SALs. Dry air is also found in SAL1 north of ~12°N. Relative humidity in the western part of SAL2 and extending southward into the region of precipitation on the north side of the low reached 60%–80% or more,³ consistent with GFS analyses (Fig. 4) and the GEOS-5 analyses and forecasts in RL1. Moving higher through the atmosphere toward the top of the SAL (Figs. 3b–f), a reversal of the temperature pattern occurs, with temperatures becoming coolest within SAL2 and warmest in the dry regions to the north and to the west of SAL2 and between the SALs. Corresponding relative humidity fields continue to show the driest air within the low-dust tongue between SAL1 and SAL2 and to the west and north of SAL2. As pointed out by Reale and Lau (2010, hereafter RL2), between ~16° and 26°N low AOD values (<0.2) extend westward into the warm and dry tongue of air. However, MODIS can provide no information about the level at which these

³ Relative humidity in the region of the wave was verified using dropsonde data from the NASA DC-8 during NAMMA on 26 August 2006.

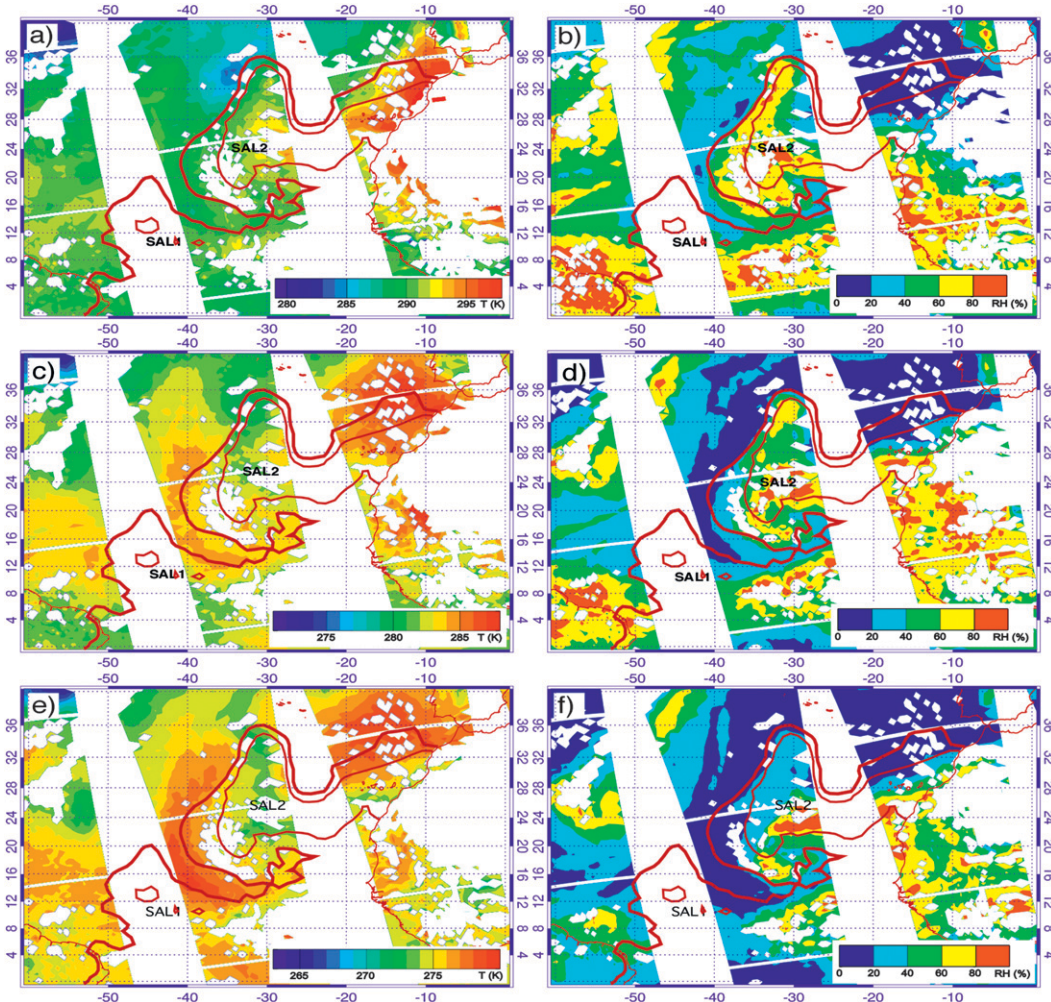


FIG. 3. Level-2 AIRS/AMSU-derived (left) temperature and (right) relative humidity from ascending orbits occurring at ~ 1330 LT 27 Aug. The coincident MODIS dust boundaries are indicated by the red lines: thick for the AOD = 0.2 contour, thin for the AOD = 0.4 contour. (left) Temperature at (a) 850, (c) 700, and (e) 600 hPa. (right) Relative humidity in the (b) 850–700-, (d) 700–600-, and (f) 600–500-hPa layers. The two SAL outbreaks discussed in the text are labeled SAL1 and SAL2. Axis labels indicate latitude and longitude values.

aerosols reside—for example, the dust could be evenly distributed in the layer or could be confined to the top, bottom, or other part of the layer—so overlap of contours of these low AOD values cannot be interpreted as indicating that the air at any given level is Saharan.⁴ Although SAL air is often slightly cooler than its

environment near its top (600–500 hPa; Carlson and Prospero 1972; Braun 2010), the presence of cooler and moister air at 700 and 600 hPa within SAL2 relative to its environment perhaps suggests less vigorous deep dry convective mixing in this air mass during its passage over the Sahara. The lack of deep heating and drying within SAL2 combined with the observation of the warmest temperatures clearly in the low-dust or nearly dust-free tongue suggests that the warming and drying in the latter feature are not related to the Sahara but are instead the result of strong subsidence-induced warming and drying.

RL2 show that the GEOS-5 analyzed warm tongue extends from $\sim 12^\circ$ to 33° N. While the warm air partially overlaps with the MODIS dust (see RL2's Figs. 1 and 2) between $\sim 18^\circ$ and 25° N, it also extends well beyond the dust region to the north and south. RL1 and RL2 fail

⁴ Ismail et al. (2010) show relative humidity profiles (see their Figs. 9 and 10) in the leading part of the dry tongue in this wave. Between approximately 1500 and 1730 UTC, an intrusion of very dry air is found between 2 and 5 km. Although they do not show the corresponding dust information, this dry air corresponded exactly with an erosion of the dust layer as dry and dust-free non-SAL air replaced the original SAL air mass in this layer, thereby lowering the AOD to ~ 0.2 – 0.3 . Therefore, the presence of low to moderate AOD values should not be viewed as evidence of SAL air throughout the layer.

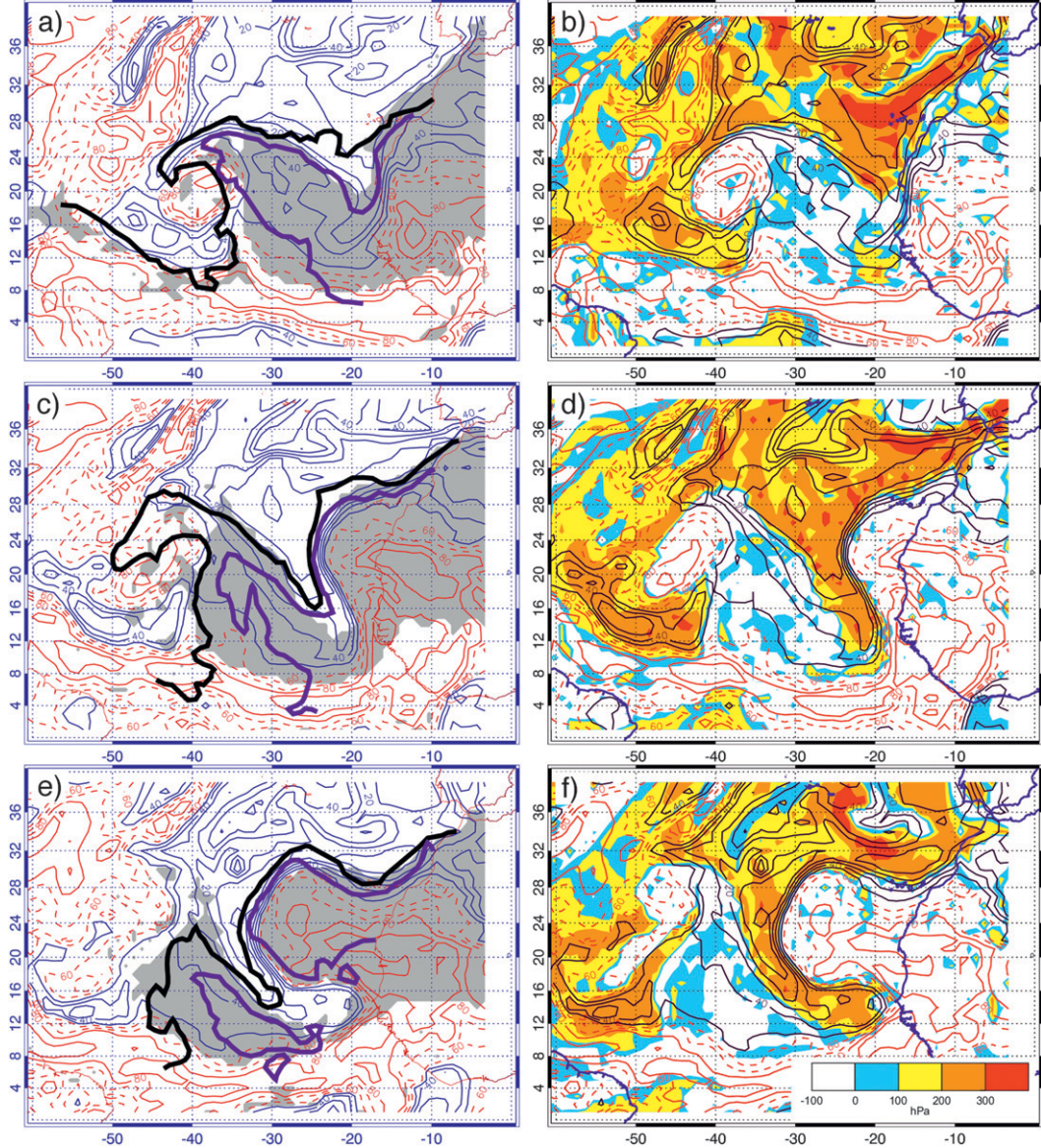


FIG. 4. Results from 6-day backward air trajectories at every grid point shown using the NCEP GFS global analyses. Trajectories were started at 1200 UTC on (top) 24 Aug, (middle) 25 Aug, and (bottom) 26 Aug at 700 hPa and run back 6 days. (a),(c),(e) Gray shading depicts locations of air parcels whose trajectories pass over the Sahara (i.e., SAL air). Blue contours show 700-hPa relative humidity $\leq 50\%$, red dashed contours 60%–70%, and red solid contours 80%–90%, with a contour interval of 10%. (b),(d),(f) Total descent (shading, hPa) occurring along the 6-day trajectories plotted at the release location of the particles. Contours are as in the left panels. The MODIS dust boundaries for each day are indicated by the boldface black line ($AOD = 0.2$) and purple line ($AOD = 0.4$). The time difference between the GFS analyses and the MODIS data is generally less than 5 h, with the latter data at the later time.

to explain how the very leading edge of SAL2 (with $AODs < 0.2$) can be warm and dry because of processes over the Sahara or radiative heating of the dust when the vast majority of SAL2 with much larger $AODs$ is much moister and cooler than the feature being discussed here. Furthermore, the analysis presented so far in this comment is based upon coincident observations from MODIS

and AIRS while RL2's Fig. 2 is based on the GEOS-5 model and MODIS AOD. Comparison of the longitude of the axis of the warm temperature anomaly in RL2's Fig. 1 (20°N , $\sim 40^{\circ}\text{W}$ at 1200 UTC 27 August) with the axis of the warm anomaly in the AIRS data in Fig. 3e (20°N , $\sim 42^{\circ}\text{W}$ at ~ 1430 UTC 27 August) suggests that the GEOS-5 model may have the feature up to 2° too far

east, thus creating a better overlap with the dust than is realistic.

The satellite data alone provide convincing evidence that the features discussed by RL1 are predominantly non-Saharan in origin. To further support this conclusion, the results of 6-day backward trajectory calculations are shown to distinguish likely SAL and non-SAL air masses and to characterize the magnitude and extent of large-scale subsidence. As shown in Fig. 9 of RL1, the thermal dipole is well depicted in the GFS analysis, although it is perhaps broader than in their GEOS-5 simulation because of resolution differences. Figure 4 (left) shows trajectory-based diagnoses of SAL air for air parcels at 700 hPa on 24–26 August. Trajectories are calculated at every grid point within the frame, with SAL air identified by whether the air parcel passes over the Sahara at any time during the trajectory. The relative humidity at the time of release of the backward trajectory (1200 UTC 24, 25, and 26 August respectively in Figs. 4a,c,e) and the MODIS dust boundaries are also shown. The two SAL air masses are well identified (cf. gray shaded areas to the MODIS-derived dust boundaries).

On 24 August, SAL1 is located over the eastern Atlantic extending from the position of Tropical Storm Debby near 40°W to the African coast, with relative humidity between 30% and 50%. SAL2 has yet to emerge from Africa. North of the dust layer is a broad pool of very dry air of non-Saharan origin. The previous day (23 August, not shown), the southern boundary of this air mass was located north of 26°N. By 24 August (Fig. 4a), this dry air has pushed southward just off the coast of Africa to approximately 20°N. By 25 August (Fig. 4c), SAL1 has moved westward, SAL2 has emerged off of Africa, and the dry non-SAL air has continued its progression southward to approximately 12°N in between the two SAL outbreaks. SAL1 has low to moderate relative humidity (~30%–50%) and SAL2 has moderate-to-high humidity (40%–90%), while the nearly dust-free tongue has extremely low humidity (<30%). By 26 August (Fig. 4e; cf. Fig. 2), the dry non-Saharan air penetrates eastward into the wave (cf. Fig. 1b), with SAL2 passing just north of the wave center. Similar patterns occur at 600 and 500 hPa (not shown), except that the dry regions become more extensive, with only a small amount of overlap with SAL air at 600 hPa. This series of trajectory-based analyses strongly suggests a southward progression of non-Saharan air into the gap between the two SAL air masses.

The right column of Fig. 4 shows the amount of descent occurring during the 6-day trajectories [i.e., $p_0 - p_{0-6}$, where p_0 and p_{0-6} are, respectively, the trajectory pressure levels at the time of release (700 hPa) of the trajectory and at the end of the trajectory 6 days earlier] plotted at the release location of the trajectory. On

24 August (Fig. 4b), the very dry air mass to the north of the dust region and extending westward around the northern side of Tropical Storm Debby is associated with a broad region of descent, whereas the dry air within SAL1 has small regions of weak descent or areas of ascent. The next two days (Figs. 4d,f) see an extension of this region of strong descent (typically greater than 100 hPa) into the gap between the two SAL outbreaks, with the descent exactly collocated with the dry tongue in the GFS analysis and the warm, dry tongue in the AIRS data. This result, coupled with the relative lack of dust within this warm and dry tongue, suggests that this feature is the result of subsidence rather than processes related to the Sahara.

While there are certainly limitations to the resolution and quality of the NCEP GFS analyses, as pointed out by RL1 and RL2, the consistency in both time and space, and with the satellite-derived fields, provides a high level of credibility to the foregoing analysis. As mentioned above, the coincident AIRS, MODIS, and CALIPSO data unambiguously indicate that the vast majority of the warm, dry tongue is in the low-dust ($AOD < 0.2$) air mass between SAL1 and SAL2. RL2 continue to rely on the GEOS-5 analyses as if they were observations. In addition, RL2 provide only a few trajectories in a very limited area at 600 hPa where SAL air appears to extend into the dry tongue. Trajectory calculations from the NCEP data (not shown) for the same time and level as in RL2 are in good agreement with RL2's findings of some intrusion of SAL air into the dry tongue at this level (and only this level). This would be consistent with the very low MODIS AOD extending into this portion of the dry tongue. However, this very small area of overlap of the SAL and dry air is dwarfed by the very broad area of descending non-SAL air seen throughout the vast majority of this warm, dry tongue. It is incredibly unlikely that the SAL contributes significantly to this feature when both the satellite data and GFS-derived trajectories suggest that the broader warm, dry tongue is of non-Saharan origin and when the SAL air mass in question (SAL2) is predominantly cool above 700 hPa and relatively moist at most levels (Fig. 3) compared to its nearby non-SAL environment. RL2 claim that radiative warming of the dust layer and cooling of the underlying boundary layer are key to the formation of the thermal dipole in the low-dust portion of the SAL despite the lack of such a feature within the very dusty air of SAL2.

4. Discussion and summary

RL1 argued that warm and dry SAL air penetrated into a promising cyclonic circulation, possibly suppressing convection and preventing development of a tropical cyclone. This conclusion was based on a reasonable set of

evidence: the warmth and dryness of the air layer, comparison to Geostationary Operational Environmental Satellite (GOES) SAL analyses (Dunion and Velden 2004), and a Hovmöller diagram that appeared to trace the dry air back to the Sahara. However, the results presented in this comment, and in Braun (2010), suggest that great care is needed in diagnosing SAL air and in attributing changes in storm intensity and evolution to the SAL. The MODIS and AIRS/AMSU satellite data and the trajectory calculations suggest that this warm, dry tongue occurred largely between two SAL air masses where dust content was low. The main driver for the warmth and dryness of this tongue of air was subsidence around and between the two SAL regions rather than processes related to the Sahara. Interestingly, the moister region north of the low pressure system that was discussed by RL1 is actually Saharan air within SAL2. The fact that the tongue of warm, dry non-SAL air also shows up readily in the GOES SAL analyses (Dunion and Velden 2004) suggests that a strict interpretation of the orange-shaded regions in the GOES analyses as SAL is problematic.

The Hovmöller diagram of relative humidity averaged between latitudes of 12° and 20°N in RL1's Fig. 1 (right) is misleading because it is unable to detect a change in the source of dry air beginning around 24 August. Prior to that time in their figure, the minimum in humidity near 8°W on 21–23 August is associated with SAL1. However, beginning on 24 August and continuing through the remainder of this event, dry air was drawn down from the area of nearly dust-free and very dry air just to the north of the SAL (Fig. 4), corresponding to the even drier anomaly in their Fig. 1 between 18° and 40°W during 24–28 August. Simple horizontal transport of SAL air westward cannot readily account for this reduction in humidity (Braun 2010). Although it appears in the Hovmöller diagram to be a single event or entity related to the SAL, a close examination of the data (Fig. 4) shows that it is not.

RL1 also suggested that cool temperatures at low levels (Fig. 3a herein and Fig. 8 of RL1) directly beneath the warm, dry air may have been the result of reduced solar heating associated with dusty air in the layer above. However, the MODIS and AIRS data clearly show that the elevated warm and dry layer and the low-level cool tongue had very low dust content. Examination of individual trajectories (not shown) suggests that this cooler low-level air originated from higher latitudes—generally from the region 30° – 40°N , 10° – 30°W , just offshore of the northwestern African and the Spanish coasts—and did not pass beneath either SAL1 or SAL2. Contrary to RL1's statement about the implausibility of simple transport explaining this cool tongue, we find that when the flow is viewed in a wave-relative reference frame (results in

the boundary layer are qualitatively similar to those at 700 hPa in Fig. 1) and through trajectory calculations, this feature is very readily explained by transport of cooler midlatitude ($>30^{\circ}\text{N}$) air southward ahead of the wave. Furthermore, the lack of substantial dust above this cool tongue suggests that reduced solar warming as a result of an elevated dust layer is not an explanation for this feature.

RL1 and RL2 suggest that the warm, dry tongue and its associated thermal dipole are very fine features, too small to be resolved by the NCEP analyses. While there is some merit to this criticism regarding the NCEP analyses, the same does not apply to the satellite observations, which clearly resolve the warm, dry tongue and the general lack of overlap with substantial aerosol. The trajectory analysis is only supplemental to our argument, used to demonstrate the role of subsidence and confirm the general non-Saharan origins of the air. The counterarguments in RL2 are focused primarily on the use of the NCEP analyses and are limited to a very small portion of the warm, dry tongue at a single level. Their response in no way rules out the predominant role of subsiding non-Saharan air.

A reliance on less direct circumstantial evidence (e.g., GOES SAL analyses instead of MODIS AOD data), incorrect assumptions linking the warm and dry air to the SAL, and a neglect of considering the role of subsidence or considering the flow in a wave-relative reference frame led RL1 to incorrectly attribute nondevelopment of a wave to the SAL. The attribution to the SAL appears to be assumed primarily because of the properties of the air mass (an elevated warm and dry air layer). However, strong subsidence can also produce marked warm and dry layers, and the prevalence of descending motion in the subtropics requires that the origin of a dry air mass never be assumed. While we do not rule out a potential role for the SAL in this event, we argue that RL1 and RL2 have failed to adequately make the case. RL1 is just one of many recent studies that have generally equated warm and dry low-to-midlevel tropical and subtropical air with the SAL and have attempted to link the SAL to a negative influence on tropical cyclone development in the Atlantic (Dunion and Velden 2004; Jones et al. 2007; Wu 2007; Dunion and Marron 2008; Shu and Wu 2009; Sun et al. 2008, 2009). The results in Braun (2010) and in this paper suggest a need for authors to conduct more thorough examinations of data, both in terms of whether air masses in question are in fact of Saharan origin and whether such air masses are the direct cause of weakening of storms.

Acknowledgments. The authors thank Karen Mohr and Jason Sippel for their helpful comments on the manuscript. This work was supported by Dr. Ramesh

Kakar at NASA Headquarters with funds from the NASA Hurricane Science Research Program.

REFERENCES

- Braun, S. A., 2010: Reevaluating the role of the Saharan Air Layer in Atlantic tropical cyclogenesis and evolution. *Mon. Wea. Rev.*, in press.
- Carlson, T. N., and J. M. Prospero, 1972: The large-scale movement of Saharan air outbreaks over the northern equatorial Atlantic. *J. Appl. Meteor.*, **11**, 283–297.
- Dunion, J. P., and C. S. Velden, 2004: The impact of the Saharan air layer on Atlantic tropical cyclone activity. *Bull. Amer. Meteor. Soc.*, **85**, 353–365.
- , and C. S. Marron, 2008: A reexamination of the Jordan mean tropical sounding based on awareness of the Saharan Air Layer: Results from 2002. *J. Climate*, **21**, 5242–5253.
- Dunkerton, T. J., M. T. Montgomery, and Z. Wang, 2009: Tropical cyclogenesis in a tropical wave critical layer: Easterly waves. *Atmos. Chem. Phys.*, **9**, 5587–5646.
- Huffman, G. J., R. F. Adler, D. T. Bolvin, G. Gu, E. J. Nelkin, K. P. Bowman, E. F. Stocker, and D. B. Wolff, 2007: The TRMM multi-satellite precipitation analysis: Quasi-global, multi-year, combined-sensor precipitation estimates at fine scale. *J. Hydrometeor.*, **8**, 38–55.
- Ismail, S., and Coauthors, 2010: LASE measurements of water vapor, aerosol, and cloud distributions in Saharan air layers and tropical disturbances. *J. Atmos. Sci.*, **67**, 1026–1047.
- Jones, T. A., D. J. Cecil, and J. Dunion, 2007: The environmental and inner-core conditions governing the intensity of Hurricane Erin (2001). *Wea. Forecasting*, **22**, 708–725.
- Reale, O., and W. K. Lau, 2010: Reply. *J. Atmos. Sci.*, **67**, 2411–2415.
- , —, K.-M. Kim, and E. Brin, 2009: Atlantic tropical cyclogenetic processes during SOP-3 NAMMA in the GEOS-5 global data assimilation and forecast system. *J. Atmos. Sci.*, **66**, 3563–3578.
- Shu, S., and L. Wu, 2009: Analysis of the influence of the Saharan air layer on tropical cyclone intensity using AIRS/Aqua data. *Geophys. Res. Lett.*, **36**, L09809, doi:10.1029/2009GL037634.
- Sun, D., K. M. Lau, and M. Kafatos, 2008: Contrasting the 2007 and 2005 hurricane seasons: Evidence of possible impacts of Saharan dry air and dust on tropical cyclone activity in the Atlantic basin. *Geophys. Res. Lett.*, **35**, L15405, doi:10.1029/2008GL034529.
- , —, —, Z. Boybeyi, G. Leptoukh, C. Yang, and R. Yang, 2009: Numerical simulations of the impacts of the Saharan air layer on Atlantic tropical cyclone development. *J. Climate*, **22**, 6230–6250.
- Wu, L., 2007: Impact of Saharan air layer on hurricane peak intensity. *Geophys. Res. Lett.*, **34**, L09802, doi:10.1029/2007GL029564.